ACS APPLIED MATERIALS & INTERFACES

Research Article

www.acsami.org

Enhanced Photoelectrochemical Solar Water Splitting Using a Platinum-Decorated CIGS/CdS/ZnO Photocathode

Mukund G. Mali,[†,‡] Hyun Yoon,[†,‡] Bhavana N. Joshi,[‡] Hyunwoong Park,[§] Salem S. Al-Deyab,[⊥] Dong Chan Lim,[*,∥] SeJin Ahn,[*,#] Carlo Nervi,[%,$] and Sam S. Yoon[*,‡]

[‡]School of Mechanical Engineering, Korea University, Seoul 136-713, Republic of Korea

[§]School of Energy Engineering, Kyungpook National University, Daegu 702-701, Republic of Korea

[⊥]Petrochemicals Research Chair, Department of Chemistry, King Saud University, Riyadh 11451, Saudi Arabia

[∥]Surface Technology Division, Korea Institute of Materials Science, Changwon 641-010, Republic of Korea

[#]Photovoltaic Laboratory, Korea Institute of Energy Research, 71-2 Jangdong, YuseongGu, DaeJeon 305-543, Republic of Korea

[%]Department of Chemistry and NIS, University of Torino, Via P. Giuria 7, 10125 Torino, Italy

[$]Interuniversity Consortium of Chemical Reactivity and Catalyis, University of Bari, 70126 Bari, Italy

Supporting Information

ABSTRACT: A $Cu(InGa)Se_2$ film was modified with CdS/ZnO for application to solar water splitting. Platinum was electrodeposited on the ZnO layer as a hydrogen evolution catalyst. The effects of the electroplating time and acidity level of the electrolyte on the photocurrent density were studied. The highest photocurrent density of −32.5 mA/cm^2 under 1.5 AM illumination was achieved with an electroplating time of 30 min at a pH of 9. This photocurrent density is higher than those reported in previous studies. The markedly high performance of the CIGS/CdS/ZnO photocathode was rationalized in terms of its type II cascade structure that facilitated efficient charge separation at the interface junction.

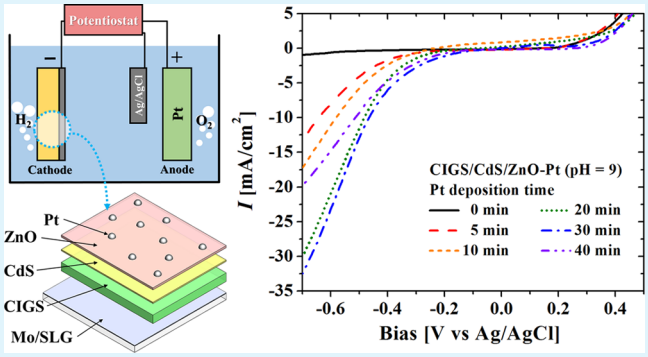

KEYWORDS: *CIGS/CdS, photocurrent, platinum, p−n junction, water splitting*

1. INTRODUCTION

Photoelectrochemical (PEC) water splitting using semiconductor electrodes is a prospective solution for reliably and sustainably harnessing carbon-free energy. For successful water splitting, the conduction band of the semiconducting material should have a greater negativity than the proton reduction potential (i.e., H^+/H_2 = 0 V), while the valence band of the material must have a greater positivity than the water oxidation potential (i.e., O_2/H_2O = +1.23 V).[1] Therefore, a thermodynamic potential of 1.23 V is required to split water. In reality, this potential must be much higher than 1.23 V because of cathodic and anodic overpotentials and losses from electrochemical reactions. Thus, this high potential requires a high material bandgap. At the same time, the bandgap of the material should be sufficiently low to imbibe the visible light spectrum for active photogeneration of electron−hole pairs.[2] Photoactive materials such as TiO_2, WO_3, ZnO, $BiVO_4$, $SrTiO_3$, Fe_2O_3, and CuO have been used for solar water splitting.[3−9]

To fully utilize sunlight, which comprises 43% visible light, there is an intense need to find visible light active PEC semiconductor materials with high efficiency and stability. Copper-based low bandgap semiconductors such as CIS, CGS, CZTS, CIGS, and CIGSS, commonly called the chalcopyrites, have recently received much attention. These species have been extensively explored for the PEC splitting of water.[10−16] Luo et al. reported the solution route for the transformation of Cu_2O into $CuInS_2$ and found a substantial decrease in the bandgap energy from 2 to 1.5 eV. This condition is attractive for water splitting because of the enhanced absorption of visible light.[2] Zheng et al. synthesized $CuInS_2$ hierarchical microstructures using a solvothermal route and utilized the resulting microstructures for photocatalytic hydrogen evolution.[13] Copper gallium sulfide, prepared by Tabata et al. using a solid-state reaction, exhibited a bandgap of 2.4 eV and was used for photocatalytic H_2 evolution analysis.[13] Rovelli et al. reported the PEC properties of CZTS photocathodes prepared by electrodeposition; they further modified these CZTS photocathodes through the deposition of CdS, AZO TiO_2, and Pt layers on CZTS and observed better electrode stability relative to bare CZTS.[16] On the other hand, Yu et al. studied the effect of platinum- and gold-doping on the photocatalytic and degradation properties of CZTS,[10] while Yokoyama et al.

Received: August 6, 2015
Accepted: September 4, 2015
Published: September 4, 2015

DOI: 10.1021/acsami.5b07267
ACS Appl. Mater. Interfaces 2015, 7, 21619−21625

studied the effect of deposition of CdS and TiO_2 on the CZTS photoelectrodes.[11] Among the chalcopyrites, $Cu(InGa)Se_2$ (CIGS) is an attractive material because CIGS has a favorable bandgap that can be tuned (between 1 to 2.4 eV) by varying the (In/Ga) ratio.[17] The deposition of metal oxide semiconductor materials with band positions compatible with those of CIGS/CdS is expected to protect the under-layer as well as promote charge extraction.

In this study, the CIGS/CdS p−n junction is modified by the deposition of an additional ZnO layer on the top. The deposition of the n-type CdS layer over the p-type CIGS layer forms a space charge (depletion) region at the solid−solid interface (p−n junction), which results in better separation of the charge carriers. Moreover, the potential difference in the valence band of the CIGS and CdS layer further enhances the charge separation.[18] Strong electric fields form at the CIGS/CdS interface, which drives the electron transport from CIGS to CdS, and the slightly positive band-offset at this interface further minimizes the interfacial recombination. Moreover, the band alignment at the CdS/ZnO interface occurs in such a way that the position of the conduction band minimum gradually decreases from CdS to ZnO, enhancing the transport of the photogenerated electrons from CIGS to ZnO. On the other hand, because ZnO has a direct bandgap of 3.3 eV, ZnO is favorable for driving the water reduction reaction[7] while maintaining suitable conduction and valence band positions. Moreover, ZnO promotes the flow of electrons from CIGS/CdS toward the electrode−electrolyte interface and the flow of holes in the opposite direction toward the collector, as illustrated in Scheme 1. Therefore, in the CIGS/CdS/ZnO

Scheme 1. Mechanism of Charge Transfer over the CIGS/CdS/ZnO-Pt Photocathode

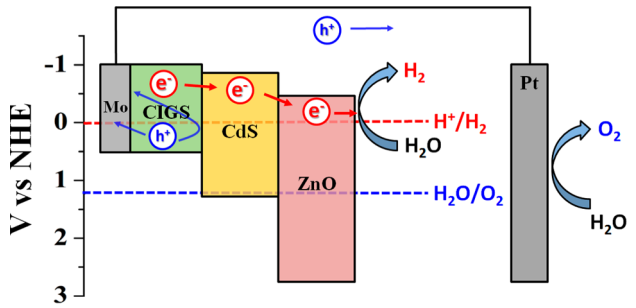

photoelectrode, the CdS layer enhances the charge carrier separation. Furthermore, the presence of the ZnO layer promotes charge migration to the electrode−electrolyte interface at which water reduction occurs. Platinum was electrodeposited over CIGS/CdS/ZnO to generate a final electrode composition of CIGS/CdS/ZnO-Pt. The effects of the Pt electrodeposition time and the electrolyte pH variation were studied to optimize the photocurrent density of the electrode fabricated herein. The effect of pH on PEC properties was also studied (pH 1, 7 and 9). Because the band bending of CIGS is relatively stiffer at pH 9, it is expected that the photocurrent onset potential shifts toward the more positive, resulting in better PEC water splitting performance.

2. EXPERIMENTAL SECTION

2.1. CIGS/CdS/ZnO-Pt Films. A 1.1−1.2 μm thick Mo thin film was direct current (DC) sputter-deposited on a soda-lime glass substrate. A three-stage process was used to grow the CIGS layers in which In, Ga, Cu, and Se were coevaporated.[19] A layer of $(In_{1-x},Ga_x)_2Se_3$ (where x = 0.3) was deposited at the first stage by coevaporating In, Ga, and Se onto the Mo/glass substrate at 400 °C. In the second stage, Cu and Se were coevaporated onto the underlying $(In,Ga)_2Se_3$ layer to form a CIGS film at 550 °C. At the end of the second stage, the Cu/(In + Ga) ratio was adjusted to 1.3 to induce CuSe liquid phase-assisted grain growth. In the third stage, In, Ga, and Se were again coevaporated to convert the composition from being Cu-rich to Cu-poor. This three-stage coevaporation process enables so-called "double-graded" engineering through which conversion efficiency improves by increasing x toward the back contact and front junction and a minimum band gap in between.

A CdS buffer layer (60 nm thick) was deposited on the CIGS films. The i-ZnO (50 nm)/n-ZnO (500 nm) bilayered films were used as a transparent conducting oxide (TCO), which was deposited on top of the CIGS/CdS film using radiofrequency (RF) magnetron sputtering. It is well-known that a thin i-ZnO layer is beneficial to mitigate the interfacial recombination at the CdS/ZnO interface.[20,21]

2.2. Electrodeposition of Platinum. To promote the electrochemical kinetics of the water reduction process, platinum dots were grown via electrodeposition in the dark from a solution of 1-mM H_2PtCl_6 in deionized water at −0.1 V versus Ag/AgCl for 5, 10, 20, 30, and 40 min.

2.3. Characterization. The crystallinity of the CIGS/CdS/ZnO-Pt films was characterized by X-ray diffraction (XRD, Rigaku, Tokyo, Japan, D/max-2500 using CuKα radiation over the 2θ range of 20°−80°). The morphology of the CIGS/CdS-Pt and CIGS/CdS/ZnO-Pt films was studied using high-resolution scanning electron microscopy (HR-SEM, S-5000, Hitachi, Japan) at 10 kV. The effective film thickness was determined by averaging five different measurements to confirm the statistical reliability. The various layers in the CIGS/CdS/ZnO film were characterized using a focused ion beam transmission electron microscope (FIB-TEM, Carl Zeiss, Auriega, Germany/TEM, JEOL) to confirm the different elements.

2.4. Photoelectrochemical Measurements. A single cell with three electrodes was used for all PEC measurements. The CIGS/CdS-Pt and CIGS/CdS/ZnO-Pt films were used as the working electrode while a Ag/AgCl rod was used as the reference electrode. A platinum wire served as the counter-electrode. These three electrodes were placed as close as possible to one another, and their positions were fixed to acquire consistent data and minimize any transport limitations in the electrolyte. A 0.5-M Na_2SO_4 (pH 1, 7, and 9) solution was the electrolyte chosen in the current study. Nitrogen gas was purged through the electrolyte solution to remove any dissolved oxygen before measurements. Artificial sunlight from a xenon arc lamp (Newport, Oriel Instruments, USA) equipped with an AM 1.5 filter was used as an irradiation source with a light intensity of 100 mW/cm^2. A potentiostat (VersaSTAT-3, Princeton Applied Research, USA) was used to record all of the photocurrent data at a scan rate of 10 mV/s. Our experimental setup is graphically described in Figure 1.

3. RESULTS AND DISCUSSION

3.1. Crystal Structure. The XRD pattern of a CIGS/CdS/ZnO-Pt film is displayed in Figure 2. A highly intense peak corresponding to the Mo substrate was observed at 40.43°. Peaks related to the (112), (220)/(204), and (312)/(116)

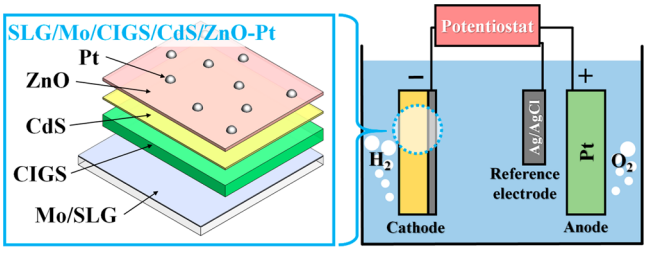

Figure 1. Schematics of the water-splitting setup.

DOI: 10.1021/acsami.5b07267
ACS Appl. Mater. Interfaces 2015, 7, 21619−21625

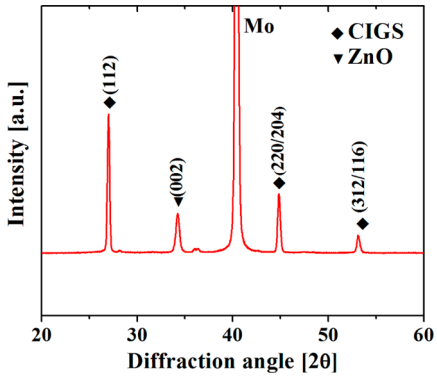

Figure 2. XRD spectrum of a CIGS/CdS/ZnO film.

planes of CIGS appeared at the respective 2θ values of 27.03, 44.84, and 53.11°. These data are in good agreement with the JCPDS file of CIGS (card no. 351102). The diffraction peak observed at 34.25°, which could be attributed to the (002) plane of ZnO, was consistent with JCPDS card no. 361451.

3.2. Morphology and Composition. The morphological features of the films were investigated by FE-SEM analysis. Figure 3 shows the cross-sectional (first column) and top (second column) views of the CIGS/CdS/ZnO films on which platinum was deposited for respective durations of 10, 20, 30, and 40 min. The cross-sectional views show an approximately 2-μm-thick CIGS layer covered with a 60 nm-thick CdS layer. The observed grain size of CIGS was 1 to 2 μm. The CIGS/CdS layers were covered with an *i*-ZnO (50 nm) layer on which a layer of *n*-ZnO (500 nm) layer was deposited. The homogeneous distribution of ZnO grains was evident from the figure. The grain size of ZnO was found to be about 0.5−1 μm. An even distribution of Pt nanoparticles over the ZnO surface was clearly visible in the SEM image. The amount of deposited Pt appeared to increase with the increasing electrodeposition time from 10 to 40 min. Notably, for 40 min of electrodeposition, relatively large grains of Pt were observed (Figure 3d), which could adversely affect the PEC performance.

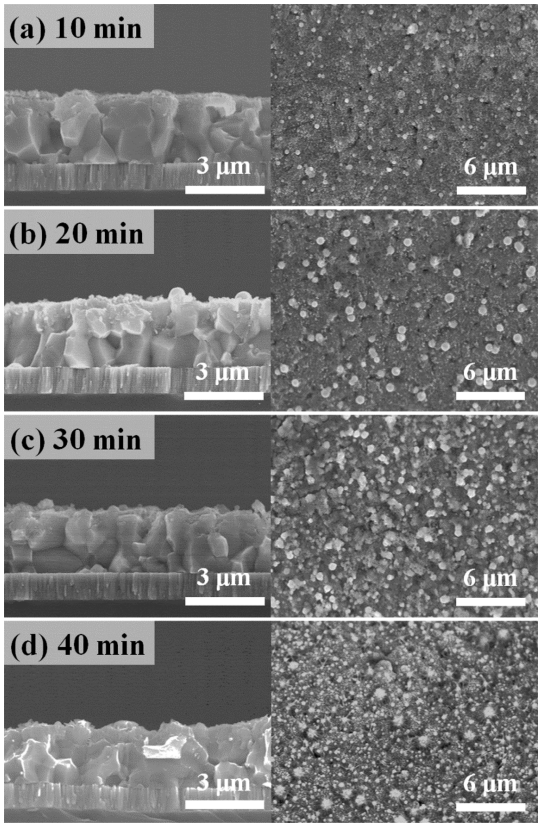

Figure 3. Cross-sectional (first column) and top (second column) views of (a) 10 min, (b) 20 min, (c) 30 min, and (d) 40 min Pt electrodeposited CIGS/CdS/ZnO films.

Figure 4 shows the cross-sectional FIB-TEM images of the CIGS/CdS/ZnO film. Here, ZnO appeared as the topmost layer with a thickness of about ∼500 nm. Below the ZnO layer, the presence of CdS was confirmed by the appearance of Cd and S. The CdS layer was about 60 nm.

3.3. Photoelectrochemical Performance. The PEC applications of the CIGS/CdS/ZnO-Pt photoelectrode were investigated systematically by varying the experimental conditions, i.e., the pH of the Na_2SO_4 electrolyte solution and the Pt electrodeposition time. The effect of the pH of the electrolyte on the PEC performance was studied at pH levels of 1, 7, and 9. The pH levels were selected to enable study of the behavior of the photoelectrodes under acidic, neutral, and basic conditions. These pH levels were achieved by adding H_2SO_4 (pH 1) or KOH (for pH 7 and 9). If the pH levels was greater than 10, the CIGS photocathode degraded because of leaching of Se as H_2Se, according to the Pourbaix diagram.[22]

The current−potential curves are displayed in Figure 5. At −0.7 V vs Ag/AgCl, the photocurrents were −10.8, −18.7, and −32.5 mA/cm^2 for pH 1, 7, and 9, respectively. When the pH of the electrolyte is 9, the photoelectrode clearly produces the best PEC performance. The photocurrent onset potential for pH levels 1 and 7 was observed at −0.5 V while that for a pH of 9 was −0.2 V; such a shift toward the right in the onset potential implies that the band bending of CIGS at pH 9 was stiffer. At pH 7 (neutral), the concentration of H^+ and OH^- was at the lowest, while H^+ ions were being consumed at the cathode. This phenomenon caused a severe gradient of the ionic concentration near the cathode, which adversely affected the water reduction rate, thereby reducing the photocurrent value.[23] At pH 1, significant photocorrosion of the photocathode was observed due to the highly acidic environment. The acid environment causes etching of the photocathode during the water-splitting reaction. As a result, a low photocurrent density was obtained at this pH level.[24]

The effect of the Pt electrodeposition time (0, 5, 10, 20, 30, and 40 min) on the photocurrent density of the CIGS/CdS/ZnO films is shown in Figure 6. The CIGS/CdS/ZnO electrode (without Pt deposition) produced a photocurrent of 0.96 mA/cm^2 with an onset potential of 0.4 V. A significant enhancement of the photocurrent of the photoelectrodes after Pt deposition was observed as the electrodeposition time increased up to 30 min. These photocurrent values were −13.5, −17.7, −30.0, and −32.5 mA/cm^2 (at −0.7 V vs Ag/AgCl) for the films electrodeposited for 5, 10, 20, and 30 min, respectively. The onset potential shifted toward the right with increasing electrodeposition time. Additionally, there was no notable improvement in the photocurrent density for electrodeposition times greater than 20 min, indicating that the 20 min film is at the saturation point. Notably, the photocurrent density decreased drastically for the 40 min film. Excessive deposition of Pt dots prevented the absorber CIGS layer from receiving sufficient light to activate electron−hole generation.

DOI: 10.1021/acsami.5b07267
ACS Appl. Mater. Interfaces 2015, 7, 21619−21625

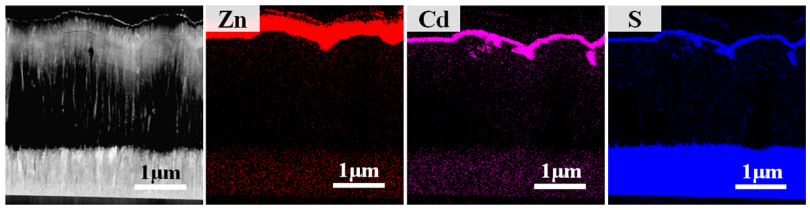

Figure 4. TEM and FIB-TEM images of the CIGS/CdS/ZnO-Pt films.

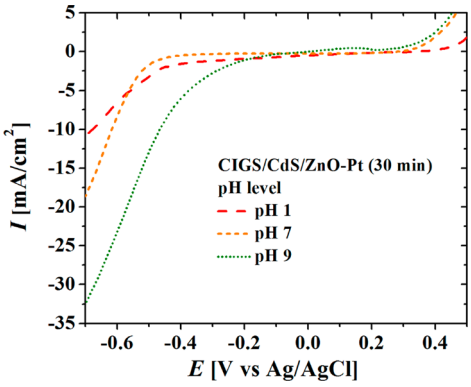

Figure 5. *I*−*V* curves for a CIGS/CdS/ZnO-Pt (30 min) film at pH levels of 1, 7, and 9 and for the film with 30 min of Pt electrodeposition (pH 9).

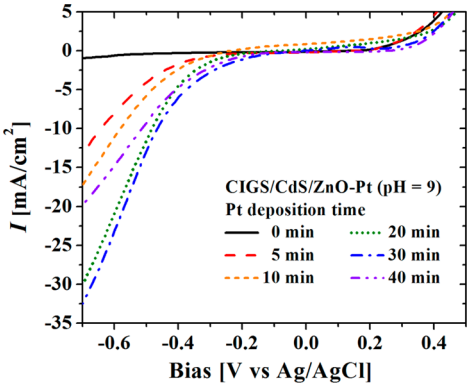

Figure 6. *I*−*V* curves for CIGS/CdS/ZnO-Pt films at 0, 5, 10, 20, 30, and 40 min of Pt electrodeposition (pH 9).

A photographic image showing the evolution of hydrogen gas over the CIGS/CdS/ZnO-Pt (20 min) photocathode upon application of a voltage is presented in Figure 7; see the movie file in the Supporting Information. The pH of the electrolyte was maintained at 9. For this film, the initial formation of bubbles started at −0.1 V. Increasing the voltage level induced the generation of larger amounts of bubbles. This qualitative observation of bubble formation was consistent with the trends observed in Figures 5 and 6.

It is well-known that CIGS without any additional layers cannot produce a high photocurrent because of the loss of electrons via recombination. These electrons drive the water reduction reaction at the electrode−electrolyte surface. Thus, CIGS alone is ineffective for driving the complete water redox reaction due to such poor electron−hole separation. To achieve better electron−hole separation, an n-type CdS layer (60 nm) was deposited over the p-type CIGS. Such a p−n junction is the most efficient way to separate the photogenerated charge carriers.[24] The resulting enhancement in the charge carrier

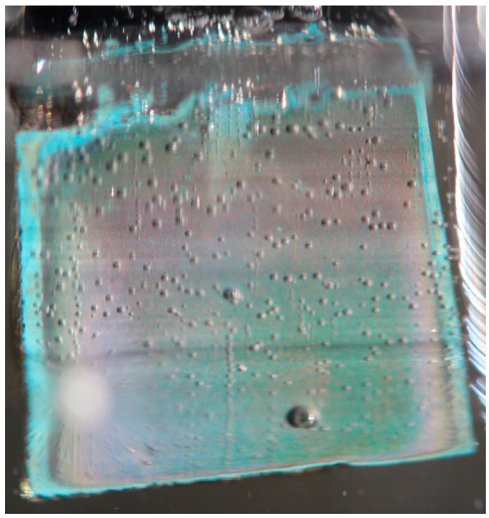

Figure 7. Image showing hydrogen evolution with the CIGS/CdS/ZnO-Pt film.

separation is attributed to the development of a depletion layer at the CIGS/CdS solid−solid interface.[18] After the electrodeposition of Pt on the CIGS/CdS film, a photocurrent density of −24 mA/cm^2 was produced, which could be further improved by installing an additional layer of ZnO that widens the overall bandgap of the multiple films. This deposition of ZnO on CIGS/CdS produced a photocurrent density of −32.5 mA/cm^2, which is the highest among comparable data documented in preceding studies.

The mechanism of hydrogen generation over the CIGS/CdS/ZnO-Pt electrode is well explained by Scheme 1. The CIGS layer drives the complete water redox reaction with the CdS layer, which increased the photocurrent density to −24 mA/cm^2. Deposition of the additional ZnO layer promotes the transport of incoming electrons from CIGS/CdS to the solid−liquid interface. Similarly, holes are transported toward the collector with minimal loss. Furthermore, the high electrical conductivity of ZnO also contributed to the highest photocurrent value of −32.5 mA/cm^2. The electron transport mechanism at the CdS/ZnO interface can be explained on the basis of the band energy levels of CdS and ZnO,[25] which is illustrated in Scheme 1.

According to the CdS−ZnO band positions, the feasibility of charge relocation from CdS to ZnO is clearly apparent because of the greater negative potential of the conduction band and valence band periphery of CdS relative to the ZnO periphery. Upon photoirradiation, electron−hole pairs are generated in the photoabsorber CIGS layer; these electrons then move to n-type CdS and n-ZnO successively, as illustrated in Scheme 1. Thus, the CIGS/CdS/ZnO electrode forms a type II cascade band structure due to the difference in chemical potential between these multiple semiconducting layers. This type II

DOI: 10.1021/acsami.5b07267
ACS Appl. Mater. Interfaces 2015, 7, 21619−21625

Table 1. Comparison of the PEC Performance of the Present CIGS/CdS/ZnO-Pt Photocathode with Previously Published Results

photocathode	electrolyte [M Na_2SO_4]	pH of electrolyte	applied potential (V vs RHE)	photocurrent density [mA/cm^2]	refs
CIGS/CdS/ZnO-Pt (30 min)	0.5	9	0.7 (Ag/AgCl)	-32.5	present work
CZTS/CdS/AZO/TiO_2−Pt	0.1	7	−0.2	−2.5	Rovelli et al.[16]
CIGS/CdS/Ti/Mo−Pt	0.5 Na_2SO_4, 0.25 M Na_2HPO_4, and 0.25 M NaH_2PO_4	6.8	0	−30.0	Kumagai et al.[28]
CIS/CdS/TiO_2−Pt	0.1 [Na_2HPO_4]	10	0	−13.0	Zhao et al.[29]
CZTS/CdS/TiO_2−Pt	0.1	9.5	0.22	−5.6	Yokoyama et al.[11]
CIGS/CdS/ZnO/Cu/-wire-/Pt	0.5		−1.1 (NHE)	−15.5	Jacobsson et al.[24]

structure causes band bending at the junction interface, facilitating the efficient transport of electrons from CIGS to ZnO.[26,27] The resulting improved electron transport led to efficient PEC performance with a photocurrent density of −32 mA/cm^2, which is the highest value recorded for comparable systems in previous studies.

The present data are compared with the previously published results in Table 1. The present photocurrent density (PCD) of −32.5 mA/cm^2 is the highest among the presented data. Kumagai et al. reported a photocurrent value of −30 mA/cm^2 using a CIGS/CdS/Ti/Mo−Pt photoelectrode; however, our photocathode consisted of CIGS/CdS/ZnO-Pt.[28] In their study, the Mo/Ti conducting layer was inserted between the CIGS/CdS layer and Pt catalyst, which greatly reduced the contact resistance. This reduced contact resistance minimizes the interfacial charge recombination, which in turn significantly improved the overall photocurrent density. Jacobsson et al. took a different approach and achieved a relatively high PCD value of −15.5 mA/cm^2 by taking advantage of the CIGS/CdS/ZnO/Cu/-wire-/Pt structure.[24] In their study, Pt-deposited FTO was used as a working electrode, and the heterojunction CIGS solar cell was placed outside of the electrolyte. As a result, the CIGS solar cell was used as a supporting battery instead of a photocathode inside the electrolyte. By avoiding direct contact between the CIGS cell and the electrolyte, Jacobsson et al. not only achieved a reasonably high photocurrent density, but they also removed the issue of cell stability against the electrolyte. However, in their system, CIGS was used simply as a supporting battery, while we used CIGS as a photocathode, in which our cell is exposed to a much harsher condition than the cell placed outside the electrolyte. Nevertheless, we achieved the highest photocurrent density value of −32.5 mA/cm^2, indicating the superiority of our heterojunction CIGS solar cell as a photocathode. In addition, we believe that the PEC performance of CIGS/CdS/ZnO could be further improved through the deposition of protective layers such as TiO_2.

Figure 8 shows the IPCE dependence of the CIGS/CdS/ZnO-Pt (30 min) photocathode on the wavelength. The IPCE data were measured in the 0.5-M Na_2SO_4 (pH 9) electrolyte solution at −0.48 V vs Ag/AgCl. The AM 1.5 filter was used during the illumination. As shown in the spectrum, the IPCE of the CIGS/CdS/ZnO-Pt (30 min) film started to increase from the wavelength of 800 nm. This increase could be attributed to the band gap energy of CIGS. The IPCE data continuously increased from 800 to 700 nm. Starting from 700 to 650 nm, the ICPE is constant and reaches its highest value of 45%. However, the IPCE data show decreased performance below

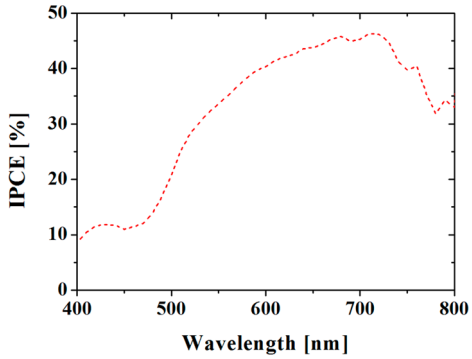

Figure 8. Incident photon-to-current efficiency (IPCE) plot of CIGS/CdS/ZnO-Pt (30 min) measured at −0.48 V vs Ag/AgCl in 0.5 M Na_2SO_4 electrolyte at pH 9.

wavelengths of 650 nm, which are related to light absorption from the additional layers, i.e., CdS and ZnO.

4. CONCLUSION

The p-type Cu(In,Ga)Se_2 films were deposited by coevaporation and modified by the deposition of an additional n-type CdS layer by chemical bath deposition and an additional ZnO layer by sputtering. The Pt electrodeposition time and the pH of the Na_2SO_4 electrolyte significantly influenced the photoelectrochemical performance. Among the studied deposited films, the CIGS/CdS/ZnO-Pt film on which Pt was electrodeposited for 30 min yielded the optimal photoelectrochemical performance with the highest photocurrent density of −32.5 mA/cm^2 (−0.7 V vs Ag/AgCl). Furthermore, the photocurrent onset potential was shifted to the positive side with increasing Pt deposition time and electrolyte pH. The enhanced PEC performance of the CIGS/CdS/ZnO-Pt photocathode can be attributed to the effective charge separation accomplished through the formation of a p−n junction at the CIGS electrode surface, along with optimal band alignment.

■ ASSOCIATED CONTENT

Supporting Information

The Supporting Information is available free of charge on the ACS Publications website at DOI: 10.1021/acsami.5b07267.

Movie S1 (AVI)

■ AUTHOR INFORMATION

Corresponding Authors

*E-mail: dclim@kims.re.kr,.

DOI: 10.1021/acsami.5b07267
ACS Appl. Mater. Interfaces 2015, 7, 21619−21625

*E-mail: swisstel@kier.re.kr,.
*E-mail: skyoon@korea.ac.kr.

Author Contributions

†M.G.M and H.Y. contributed equally.

Notes

The authors declare no competing financial interest.

■ ACKNOWLEDGMENTS

This research was supported by Global Frontier Program through the Global Frontier Hybrid Interface Materials (GFHIM) of the National Research Foundation of Korea (NRF) funded by the Ministry of Science, ICT & Future Planning (2013M3A6B1078879). This work was also supported by NRF-2013R1A2A2A05005589 and by the Industrial Strategic Technology Development Program (10045221) funded by the Ministry of Knowledge Economy (MKE, Korea). The authors extend their appreciation to the Deanship of Scientific Research at King Saud University for its funding this Prolific Research group (PRG-1436-03). The first author is grateful for the financial support made by a Korea University Grant.

■ REFERENCES

(1) Hisatomi, T.; Kubota, J.; Domen, K. Recent Advances in Semiconductors for Photocatalytic and Photoelectrochemical Water Splitting. *Chem. Soc. Rev.* **2014**, *43* (22), 7520−7535.
(2) Luo, J.; Tilley, S. D.; Steier, L.; Schreier, M.; Mayer, M. T.; Fan, H. J.; Grätzel, M. Solution Transformation of Cu_2O into $CuInS_2$ for Solar Water Splitting. *Nano Lett.* **2015**, *15* (2), 1395−1402.
(3) Yoon, H.; Mali, M. G.; Choi, J.-Y.; Kim, M.-w.; Choi, S. K.; Park, H.; Al-Deyab, S. S.; Swihart, M. T.; Yarin, A. L.; Yoon, S. S. Nanotextured Pillars of Electrosprayed Bismuth Vanadate for Efficient Photoelectrochemical Water Splitting. *Langmuir* **2015**, *31* (12), 3727−3737.
(4) Yoon, H.; Mali, M. G.; Kim, M.-w.; Al-Deyab, S. S.; Yoon, S. S. Electrostatic Spray Deposition of Transparent Tungsten Oxide Thin-film Photoanodes for Solar Water Splitting. *Catal. Today* **2015**, DOI: 10.1016/j.cattod.2015.03.037.
(5) Patil, K.; Sathaye, S.; Khollam, Y.; Deshpande, S.; Pawaskar, N.; Mandale, A. Preparation of TiO_2 Thin Films by Modified Spin-coating Method using an Aqueous Precursor. *Mater. Lett.* **2003**, *57* (12), 1775−1780.
(6) Mali, M. G.; Yoon, H.; Kim, M.-w.; Swihart, M. T.; Al-Deyab, S. S.; Yoon, S. S. Electrosprayed Heterojunction $WO_3/BiVO_4$ Films with Nanotextured Pillar Structure for Enhanced Photoelectrochemical Water Splitting. *Appl. Phys. Lett.* **2015**, *106* (15), 151603.
(7) Paracchino, A.; Laporte, V.; Sivula, K.; Grätzel, M.; Thimsen, E. Highly Active Oxide Photocathode for Photoelectrochemical Water Reduction. *Nat. Mater.* **2011**, *10* (6), 456−461.
(8) Sivula, K.; Le Formal, F.; Grätzel, M. Solar Water Splitting: Progress using Hematite (α-Fe_2O_3) Photoelectrodes. *ChemSusChem* **2011**, *4* (4), 432−449.
(9) Iwashina, K.; Kudo, A. Rh-doped $SrTiO_3$ Photocatalyst Electrode Showing Cathodic Photocurrent for Water Splitting under Visible-light Irradiation. *J. Am. Chem. Soc.* **2011**, *133* (34), 13272−13275.
(10) Yu, X.; Shavel, A.; An, X.; Luo, Z.; Ibáñez, M.; Cabot, A. Cu_2ZnSnS_4-Pt and Cu_2ZnSnS_4-Au Heterostructured Nanoparticles for Photocatalytic Water Splitting and Pollutant Degradation. *J. Am. Chem. Soc.* **2014**, *136* (26), 9236−9239.
(11) Yokoyama, D.; Minegishi, T.; Jimbo, K.; Hisatomi, T.; Ma, G.; Katayama, M.; Kubota, J.; Katagiri, H.; Domen, K. H_2 Evolution from Water on Modified Cu_2ZnSnS_4 Photoelectrode under Solar Light. *Appl. Phys. Express* **2010**, *3* (10), 101202.
(12) Tabata, M.; Maeda, K.; Ishihara, T.; Minegishi, T.; Takata, T.; Domen, K. Photocatalytic Hydrogen Evolution from Water using Copper Gallium Sulfide under Visible-light Irradiation. *J. Phys. Chem. C* **2010**, *114* (25), 11215−11220.
(13) Zheng, L.; Xu, Y.; Song, Y.; Wu, C.; Zhang, M.; Xie, Y. Nearly Monodisperse $CuInS_2$ Hierarchical Microarchitectures for Photocatalytic H_2 Evolution under Visible Light. *Inorg. Chem.* **2009**, *48* (9), 4003−4009.
(14) Dhere, N. G. Present Status and Future Prospects of CIGSS Thin Film Solar Cells. *Sol. Energy Mater. Sol. Cells* **2006**, *90* (15), 2181−2190.
(15) Naghavi, N.; Spiering, S.; Powalla, M.; Cavana, B.; Lincot, D. High-efficiency Copper Indium Gallium Diselenide (CIGS) Solar Cells with Indium Sulfide Buffer Layers Deposited by Atomic Layer Chemical Vapor Deposition (ALCVD). *Prog. Photovoltaics* **2003**, *11* (7), 437−443.
(16) Rovelli, L.; Tilley, S. D.; Sivula, K. Optimization and Stabilization of Electrodeposited Cu_2ZnSnS_4 Photocathodes for Solar Water Reduction. *ACS Appl. Mater. Interfaces* **2013**, *5* (16), 8018−8024.
(17) Yoon, H.; Na, S. H.; Choi, J. Y.; Kim, M. W.; Kim, H.; An, H. S.; Min, B. K.; Ahn, S.; Yun, J. H.; Gwak, J.; Yoon, K.; Kolekar, S. S.; van Hest, M. F. A. M.; Al-Deyab, S. S.; Swihart, M. T.; Yoon, S. S. Carbon- and Oxygen-Free Cu(InGa) $(SSe)_2$ Solar Cell with a 4.63% Conversion Efficiency by Electrostatic Spray Deposition. *ACS Appl. Mater. Interfaces* **2014**, *6* (11), 8369−8377.
(18) Moriya, M.; Minegishi, T.; Kumagai, H.; Katayama, M.; Kubota, J.; Domen, K. Stable Hydrogen Evolution from CdS-modified $CuGaSe_2$ Photoelectrode under Visible-light Irradiation. *J. Am. Chem. Soc.* **2013**, *135* (10), 3733−3735.
(19) Jung, S.; Ahn, S.; Yun, J. H.; Gwak, J.; Kim, D.; Yoon, K. Effects of Ga Contents on Properties of CIGS Thin Films and Solar Cells Fabricated by Co-evaporation Technique. *Curr. Appl. Phys.* **2010**, *10* (4), 990−996.
(20) Misic, B.; Pieters, B.; Theisen, J.; Gerber, A.; Rau, U. Shunt Mitigation in ZnO: Al/i-ZnO/CdS/Cu(In, Ga)Se_2 Solar Modules by the i-ZnO/CdS Buffer Combination. *Phys. Status Solidi A* **2015**, *212* (3), 541−546.
(21) Rau, U.; Schmidt, M. Electronic Properties of ZnO/CdS/Cu(In, Ga)Se_2 Solar Cells—Aspects of Heterojunction Formation. *Thin Solid Films* **2001**, *387* (1), 141−146.
(22) Savadogo, O. Chemically and Electrochemically Deposited Thin Films for Solar Energy Materials. *Sol. Energy Mater. Sol. Cells* **1998**, *52* (3), 361−388.
(23) Yokoyama, D.; Minegishi, T.; Maeda, K.; Katayama, M.; Kubota, J.; Yamada, A.; Konagai, M.; Domen, K. Photoelectrochemical Water Splitting using a Cu(In, Ga)Se_2 Thin Film. *Electrochem. Commun.* **2010**, *12* (6), 851−853.
(24) Jacobsson, T. J.; Platzer-Björkman, C.; Edoff, M.; Edvinsson, T. $CuIn_xGa_{1-x}Se_2$ as an Efficient Photocathode for Solar Hydrogen Generation. *Int. J. Hydrogen Energy* **2013**, *38* (35), 15027−15035.
(25) Sim, H.; Lee, J.; Cho, S.; Cho, E.-S.; Kwon, S. J. A Study on the Band Structure of ZnO/CdS Heterojunction for CIGS Solar-Cell Application. *Semicond. Sci. Technol.* **2015**, *15* (2), 267−275.
(26) Wang, Y.; Wang, Q.; Zhan, X.; Wang, F.; Safdar, M.; He, J. Visible Light Driven Type II Heterostructures and Their Enhanced Photocatalysis Properties: A Review. *Nanoscale* **2013**, *5* (18), 8326−8339.
(27) Choi, Y.; Beak, M.; Yong, K. Solar-driven Hydrogen Evolution Using a $CuInS_2$/CdS/ZnO Heterostructure Nanowire Array as an Efficient Photoanode. *Nanoscale* **2014**, *6* (15), 8914−8918.
(28) Kumagai, H.; Minegishi, T.; Sato, N.; Yamada, T.; Kubota, J.; Domen, K. Efficient Solar Hydrogen Production from Neutral Electrolytes using Surface-modified Cu(In, Ga)Se_2 Photocathodes. *J. Mater. Chem. A* **2015**, *3* (16), 8300−8307.
(29) Zhao, J.; Minegishi, T.; Zhang, L.; Zhong, M.; Gunawan; Nakabayashi, M.; Ma, G.; Hisatomi, T.; Katayama, M.; Ikeda, S.; Shibata, N.; Yamada, T.; Domen, K. Enhancement of Solar Hydrogen Evolution from Water by Surface Modification with CdS and TiO_2 on Porous $CuInS_2$ Photocathodes Prepared by an Electrodeposition-

DOI: 10.1021/acsami.5b07267
ACS Appl. Mater. Interfaces 2015, 7, 21619−21625

Sulfurization Method. *Angew. Chem., Int. Ed.* **2014**, *53* (44), 11808−11812.

DOI: 10.1021/acsami.5b07267
ACS Appl. Mater. Interfaces 2015, 7, 21619−21625